Analysis of Magnetic Forces and Vibration in a Converter-Fed Synchronous Hydrogenerator

Mostafa Valavi, Arne Nysveen, Roy Nilsen
Norwegian University of Science and Technology (NTNU)
Trondheim, Norway
mostafa.valavi@ntnu.no

Jean Le Besnerais, Emile Devillers
EOMYS Engineering
Lille-Hellemmes 59260, France
jean.lebesnerais@eomys.com

***Abstract*—This paper investigates the influence of converter-fed operation on magnetic forces and radial vibration in a hydrogenerator. Flux density distribution is computed using time-stepping finite element (FE) analysis and used to calculate force density distribution based on Maxwell stress tensor. Both temporal and spatial characteristics of selected flux density and force density waves are studied. Important spatial harmonics of radial forces are investigated and compared for converter-fed and converter-less operations. Vibration analysis is also presented based on the magnetic field data computed by FE analysis.**

***Keywords*—Hydrogenerator, fractional-slot windings, PWM converter, radial forces, vibration, pumped-storage hydro.**

I. INTRODUCTION

In a conventional hydropower plant, synchronous generator is directly connected to the grid, meaning that its rotational speed and electrical frequency must remain constant. However, there are applications where variable-speed operation of hydropower plant can be advantageous [1]. For example, in a pumped-storage plant, in order to adjust the pumping power, rotational speed of the motor-generator and pump-turbine needs to be varied. To realize such a variable-speed system, two electrical configurations can be employed using either a doubly-fed induction machine (DFIM) or converter-fed synchronous machine (CFSM) [1, 2]. CFSM system has distinct advantages over DFIM configuration [3], but the main drawback is the need for a full-power converter. On the other hand, the size of the converter in a DFIM system is up to 30% of the rated power. Because of this, DFIM system has been the preferred configuration in high power applications (above 100 MW). However, with the advancements in the field of semiconductor devices and converter topologies, converters with higher power ratings will be available in future, making CFSM an interesting choice even for high power applications [1, 3]. In addition to pumped-storage plants, a CFSM system can be used in HVDC-connected [4] and also small hydropower [5] plants.

Variable-speed operation of hydropower plants can offer many benefits both to the power system and to the plant itself. With adjusting pumping power, the pumped-storage plant can contribute to frequency regulation in pumping mode. This feature enables pumped-storage plant to play an important role in a power system with high penetration of renewable sources. As a large energy storage system, it can compensate the variable production of renewables. For the hydropower plant, variable speed operation can lead to a higher hydraulic efficiency and lower vibration and cavitation problems in the hydraulic machinery [1, 6].

TABLE I
SPECIFICATIONS OF HYDROGENERATOR AND CONVERTER

Generator	Power	105 MVA
	Speed	428.6 rpm
	Number of poles	14
	Number of slots	180
	Airgap diameter	3672 mm
	Machine length	1800 mm
Converter	Configuration	2-level VSC
	Switches	Ideal
	PWM	Sinusoidal
	Carrier frequency	450 Hz, 1050 Hz

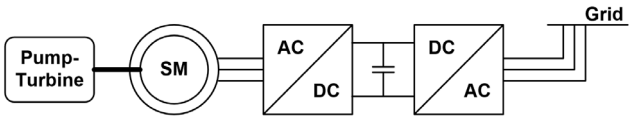

Fig. 1. CFSM configuration in a pumped-storage hydropower plant.

The focus of this paper is on the hydrogenerator in a CFSM system (as shown in Fig. 1). Converter-Fed operation of a synchronous generator can bring new challenges (e.g. increased level of losses and vibration). This paper investigates magnetic forces acting on the stator teeth (i.e. main source of magnetic vibration) in a hydrogenerator connected to a PWM converter. For converter-fed operation, two carrier frequencies are considered, i.e. 1050 Hz and 450 Hz. The electromagnetic results are compared with a conventional case where the generator supplies a resistive load. The power electronic converter is modeled in an electrical circuit coupled with time-stepping FE analysis, where the hydrogenerator is modeled. Vibration analysis is presented for the case of 1050 Hz carrier frequency. Details of electromagnetic FE modeling and simulation are discussed in Section II. Analysis of magnetic field and radial forces are presented in Sections III and IV

This work was supported by Norwegian Hydropower Centre (NVKS) and Norwegian Research Centre for Hydropower Technology (HydroCen).

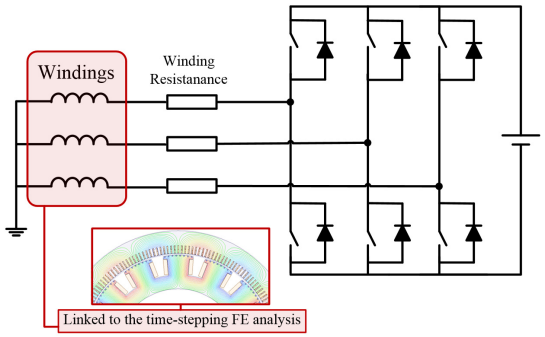

Fig. 2. Coupled circuit (2-level converter) linked to the electromagnetic FE simulations.

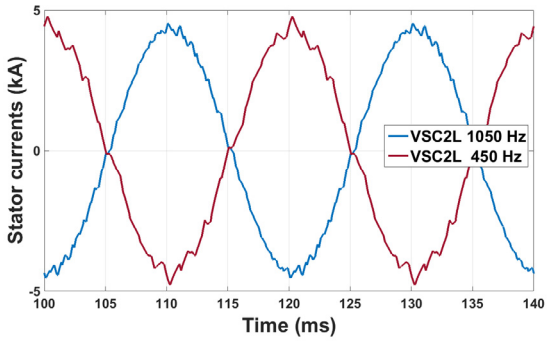

Fig. 3. Generator terminal current in converter-fed operation with two different carrier frequencies.

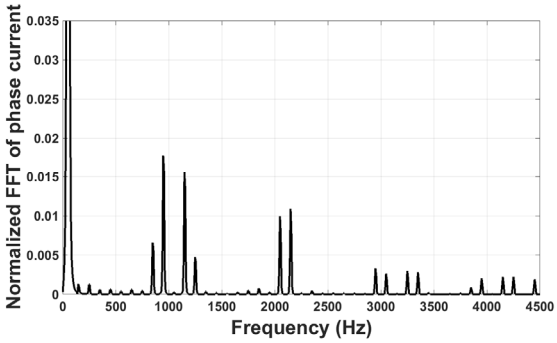

Fig. 4. Time harmonic content of terminal current in the case of 1050 Hz carrier frequency.

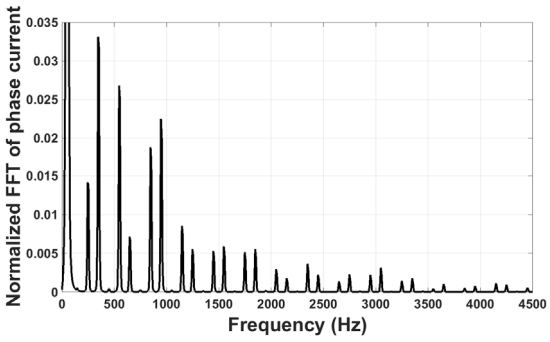

Fig. 5. Time harmonic content of terminal current in the case of 450 Hz carrier frequency.

respectively. Vibration analysis is included in Section V. Section VI presents the concluding remarks.

II. Time-Stepping Electromagnetic FE Simulations

In order to investigate both spatial and temporal harmonics of magnetic flux density and force density, time stepping FE analysis is employed. Field data (i.e. flux density distribution in the airgap) are stored in every time step and then are used for the calculation of radial and tangential force density based on Maxwell stress tensor. Since the simulation includes a power electronic circuit, a sufficiently small time step (10 microseconds) is used. Due to computational considerations, PWM converter is modeled as simple as possible. A two-level voltage source converter (as the machine-side converter) with ideal switches and sinusoidal PWM is used as shown in Fig. 2. As can be seen in the figure, only machine side converter is modeled. Converter is connected to a DC source, which is a simple representation of the DC link capacitor connected to the grid side converter. Specifications of the hydrogenerator and PWM converter are presented in Table I. The hydrogenerator under study is a 14-pole/180-slot machine with fractional-slot windings. Damper bars are not modeled. It is possible to have a converter-fed synchronous generator without dampers since the transient operation can be controlled by the power electronic converter. However, the converter cannot be bypassed if generator has no damper bars. The carrier frequency is set to be 1050 Hz and 450 Hz. It should be noted that this two-level topology is not the preferred converter for such a high power application. However, it fulfils the aim of this paper, which is to investigate how additional harmonics (specifically well-known switching harmonics) in the stator current due to the converter-fed operation affect the flux density and force density harmonics in the hydrogenerator. In [7], electromagnetic analysis of the same hydrogenerator connected to a NPC (neutral-point-clamped) converter is presented.

Fig. 3 shows stator current waveform in the case of converter-fed operation, with 1050 Hz and 450 Hz as the carrier frequency. As can be seen in the figure, currents are distorted having higher order temporal harmonics produced by switching. Temporal harmonics of the hydrogenerator current (normalized to the fundamental 50 Hz harmonic) are depicted in Fig. 4 and Fig. 5 for 1050 Hz and 450 Hz cases, respectively. It should be noted that even though the terminal voltages contain harmonics with a relatively high amplitude due to the converter-fed operation, current waveforms are significantly less distorted and amplitude of the additional harmonics is greatly reduced. This is because the machine itself has a relatively large inductance. The dominant additional harmonics produced by switching are $f_{PWM} \pm 2f_s$ harmonics (i.e. 1150 Hz and 950 Hz in the case of 1050 Hz carrier frequency, 550 Hz and 350 Hz in the case of 450 Hz carrier frequency) followed by $2f_{PWM} \pm f_s$ harmonics (i.e. 2150 Hz and 2050 Hz in the case of 1050 Hz carrier frequency, 950 Hz and 850 Hz in the case of 450 Hz carrier frequency). This is as expected for this 2-level PWM converter. As mentioned earlier, carrier frequency (f_{PWM}) is either 1050 Hz or 450 Hz and electrical frequency (f_s) is 50 Hz.

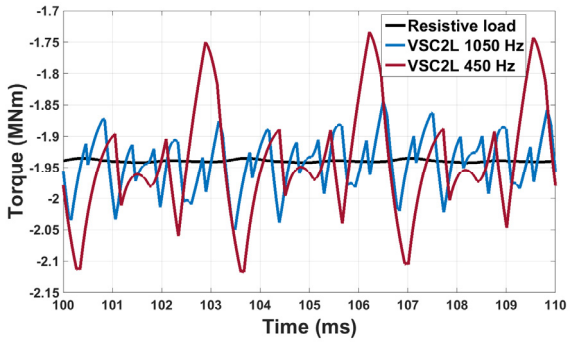

Fig. 6. Electromagnetic torque in different loading cases.

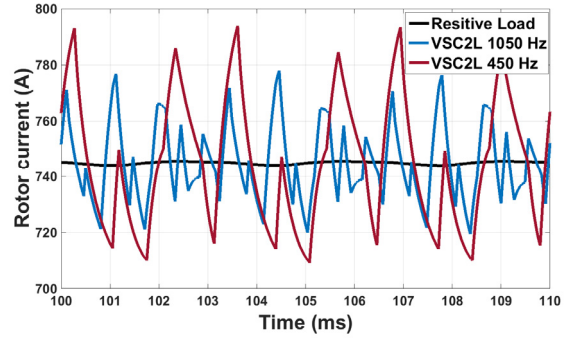

Fig. 7. Rotor field current in different loading cases.

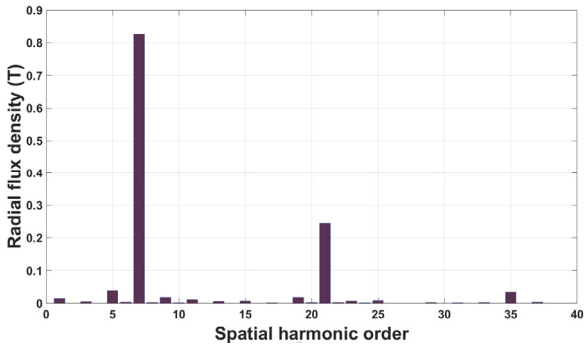

Fig. 8. Spatial harmonic content of radial flux density in one time instant.

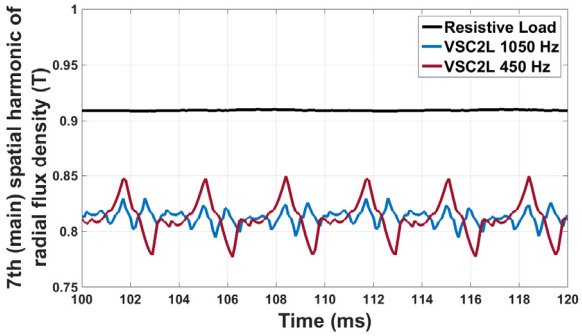

Fig. 9. Time-varying amplitude of the 7th (main) spatial harmonic of radial flux density.

Comparing Fig. 4 and Fig. 5, it is evident that, as expected, the amplitude of the additional harmonics is larger in the case of lower carrier frequency. The amplitude of the largest harmonic caused by switching is 1.8% and 3.3% of fundamental 50 Hz component in the case of 1050 Hz and 450 Hz carrier frequencies, respectively. Additional time harmonics produced by switching can also be seen in the torque and rotor field current of the generator, as shown in Fig. 6 and Fig. 7. For comparison, a converter-less hydrogenerator supplying a resistive load is also simulated. For both converted-fed and converter-less cases, the magnitudes of the rotor field current, stator current and the electromagnetic torque are almost equal.

III. Analysis of Magnetic Field

In order to investigate characteristics of the radial forces, the first step is to study flux density temporal and spatial harmonics. A magnetic flux density wave (radial component for instance) in the airgap can be generally expressed as:

$$B_r(\theta,t) = B_{rm}\cos\left(h\theta - k_B\omega t - \varphi_B\right) \qquad (1)$$

where θ and t are angular mechanical position and time, h and k_B denote spatial and temporal harmonics. ω and φ_B are angular velocity and phase, respectively. Fig. 8 shows spatial harmonic orders of radial flux density in one time instant, in the case of resistive load. As can be seen in the figure, the main harmonic is the 7th, corresponding to the pole pair number. Two other important harmonics (from the perspective of generating an important radial force harmonic) are 5th and 9th harmonics. As will be discussed in the next section, the interaction between these three harmonics produces a force wave of order 2 and consequently lowest non-zero mode of vibration.

Even though Fig. 8 can be effectively used to identify the major spatial harmonics contributing to produce dominant vibrational radial forces, it does not reveal any information about the temporal harmonic content of each spatial harmonics. This information is specifically useful in the case of converter-fed operation where additional time harmonics are produced due to the switching.

A typical case in converter-fed synchronous machines is the production of a flux density wave with the same spatial order as the fundamental, but with a frequency around the switching frequency [8]. The main spatial harmonic itself (i.e. 7th for this hydrogenerator) has a frequency equal to the fundamental frequency (i.e. 50 Hz here). In Section III and Section IV, to be able to study both temporal and spatial characteristics of the flux density and radial force density distributions, the time-varying amplitude and phase shift of each spatial harmonic are investigated. Having a constant amplitude for a spatial harmonic over time means that it contains only one temporal harmonic, while a time-varying amplitude is an indication of additional temporal harmonics. Two waves of same spatial

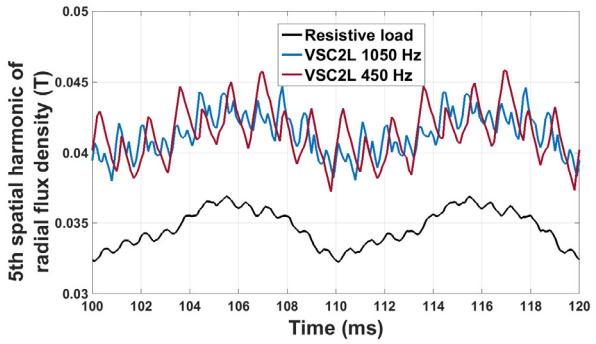

Fig. 10. Time-varying amplitude of the 5th spatial harmonic of radial flux density.

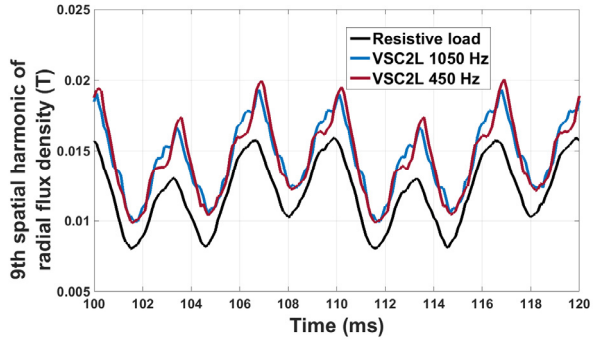

Fig. 11. Time-varying amplitude of the 9th spatial harmonic of radial flux density.

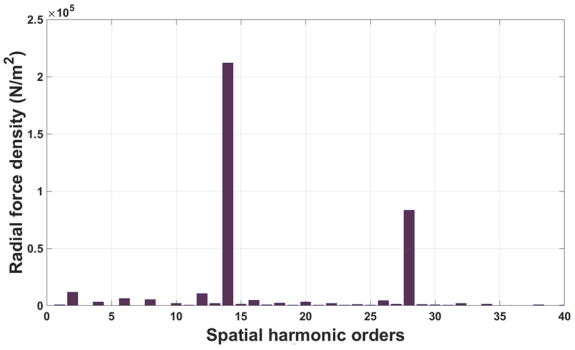

Fig. 12. Spatial harmonic content of radial force density in one time instant.

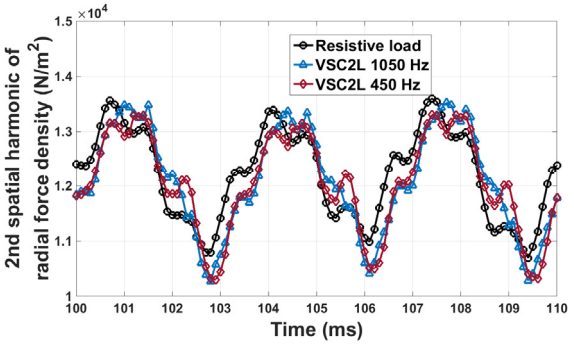

Fig. 13. Time-varying amplitude of the 2nd spatial harmonic of radial force density.

order but different temporal harmonics rotate with different speed in the airgap (hence relative phase shift is not constant), leading to a time-varying amplitude for that spatial order.

Fig. 9 shows the amplitude of the main harmonic (7th) in both converter-fed and resistive loading cases. While the amplitude is almost constant in the case of resistive loading, it is evident that converter-fed operation generates additional temporal harmonics of this main spatial component. Variations in the amplitude are mainly caused by the additional switching harmonics in the current waveform (discussed in Section II) and are considerably larger in the case of 450 Hz carrier frequency. Time-varying amplitude of the 5th and 9th spatial harmonic orders are depicted in Fig. 10 and Fig. 11. According to the figures, these two spatial harmonics also contain temporal harmonics but they are less influenced by the converter-fed operation, compared with the main 7th harmonic. Analysis of the time-varying phase shift of these three spatial harmonics (not included in the paper) reveals that the dominant temporal harmonic of 5th and 7th component is 50 Hz, while the dominant frequency for 9th spatial order is 150 Hz.

IV. Analysis of Radial Forces

Radial magnetic forces are among the main causes of vibration in rotating electrical machines. In this paper, Maxwell stress tensor is employed to calculate the radial force density based on the numerically computed flux density distribution in the airgap:

$$f_r = \frac{1}{2\mu_0}\left(B_r^2 - B_t^2\right) \tag{2}$$

In the equation above B_r and B_t denote radial and tangential components of radial flux density in the airgap. Radial force waves acting on the stator are functions of both time and space and can be written as:

$$f_r(\theta, t) = F_{rm} \cos\left(r\theta - k_F \omega t - \varphi_F\right) \tag{3}$$

where k_F denote temporal harmonic and r is the spatial harmonic order (also known as mode number). The magnitude of the deformations in the stator is inversely proportional the mode number. This means that the lower the spatial order of the radial force wave, the higher the amplitude of the vibrations (resonance is neglected). This is why low spatial orders of radial force density are the most important harmonics from vibration perspective. Fig. 12 shows the spatial harmonic orders of radial force density in one time instant. As can be seen in the figure, the order of the lowest order harmonic is 2, equal to the greatest common divisor (GCD) of pole and slot numbers. According to (2), this lowest order is produced by the interaction between flux density harmonics which their spatial orders differ by two. Based on Fig. 8, it can be shown that 2nd mode is produced by the interaction between 5th and 7th harmonics and also 7th and 9th harmonics of flux density. Time-varying amplitude of 2nd

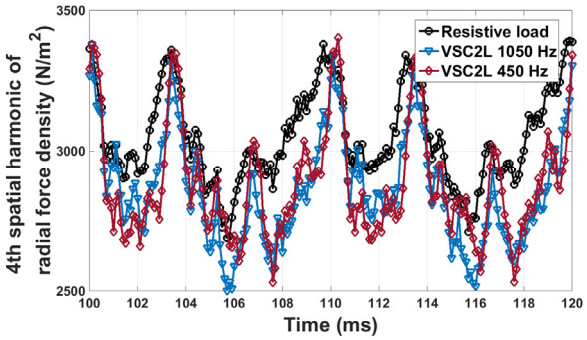

Fig. 14. Time-varying amplitude of the 4th spatial harmonic of radial force density.

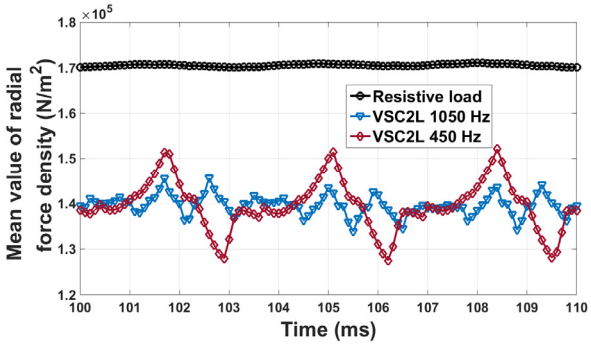

Fig. 15. Time-varying mean value of radial force density distribution (0th order forces).

TABLE II
ELASTIC PROPERTIES OF LAMINATION M400-50A

Young modulus [MPa]		Shear modulus [MPa]		Poisson ratio	
E_x	215	G_{xy}	82.7	ν_{xy}	0.3
E_y	215	G_{yz}	2	ν_{yz}	0.03
E_z	80	G_{zx}	2	ν_{zx}	0.03

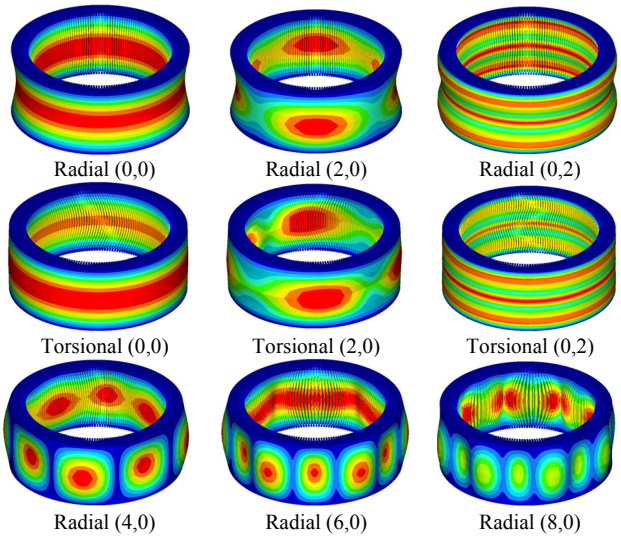

Fig. 16. Illustations of radial and torsional modes (m,n).

and 4th spatial radial force harmonics are depicted in Fig. 13 and Fig. 14 for both cases of converter-fed and resistive loadings. Since the amplitude does not remain constant over time, more than one time harmonic exist for each spatial mode. According to Fig. 13, it can be seen that converter-fed operation does not considerably change the characteristics of the 2nd order force, which is potentially important from vibration perspective. Similarly, Fig. 14 shows that the 4th force harmonic is not affected considerably as well. According to (2), the expected fundamental frequency of the 2nd mode is twice the electrical frequency (i.e. 100 Hz). This can be verified by checking the time-varying phase shift of this spatial harmonic as explained in Section III. Variations in the amplitude of the 2nd radial force component do exist in the case of resistive load and are not related to the converter-fed operation. These variations are caused by the interaction between the following two flux density waves: 7th spatial harmonic with the frequency of 50 Hz and 9th spatial harmonic with the frequency of 150 Hz.

In addition to the 2nd mode, 0th mode of vibration is also investigated because in presence of additional time harmonics, this mode could be of importance. The 0th spatial order (i.e. mean value of radial force density) is produced by flux density waves of same spatial order but different temporal harmonics. Fig. 15 clearly shows that 0th order radial force is intensified in the case of converter-fed operation.

V. VIBRATION ANALSYIS

In this section, vibration characteristics are investigated for the converter-fed hydrogenerator, in the case of 1050 Hz carrier frequency. The vibration analysis is based on the flux density distribution computed by time-stepping electromagnetic FE analysis (presented in Section III).

A. Principle

The stator mechanical response to the magnetic forces is computed using the electromagnetic vibration synthesis (EVS) technique [9]. The stator mechanical response is assumed to be linear and can be obtained by summing the complex magnitude of each harmonic force (f,r) weighted by its frequency response function (FRF). The FRF is the displacement of the stator yoke under a unit magnitude rotating force wave (f,r) applied on the teeth, it includes the effect of the structural modes on the dynamic mechanical response. Here, each FRF is computed by using the automated coupling between MANATEE [10] and the FE software Hypermesh/Optistruct. The coupling consists in automatically generating both CAD and mesh of the stator in Hypermesh, so that the user can directly run the solver Optistruct, re-import the results in MANATEE and finally perform the EVS to get the overall vibration level including modal contribution.

B. Stator modal analysis

A stator modal analysis is performed in Optistruct to obtain the main structural modes of the machine. For the sake of simplicity, the stator is here modelled without frame, in clamped-clamped boundary conditions (null displacement at both ends), and the stator windings are modelled as a distributed mass in the slots. The number of axial layers is 8 which makes

TABLE III
STRUCTURAL MODES

Radial (yoke deflection)		Tangential (pure tooth bending)	
Mode(m,n)	*Frequency [Hz]*	*Mode(m,n)*	*Frequency [Hz]*
(0,0)	367	(0,0)	131
(2,0)	134	(0,2)	421
(4,0)	220	(2,0)	790
(6,0)	417		
(8,0)	670		
(10,0)	930		
(0,2)	550		
(0,4)	876		

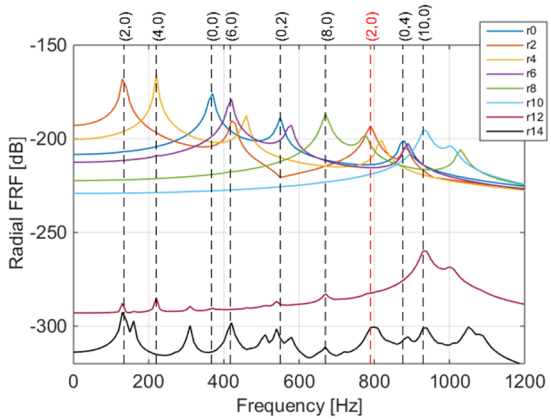

Fig. 17. Radial FRF of the stator yoke due to radial unit wave force of even orders from r=0 to r=14.

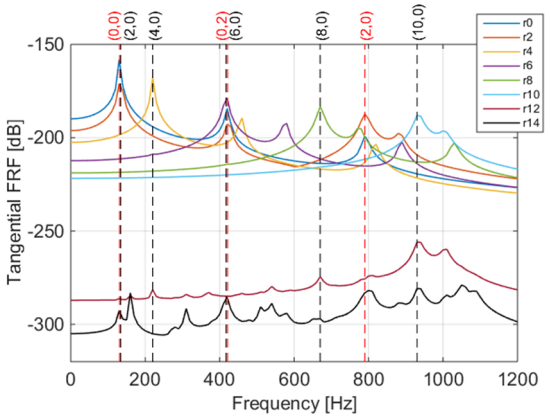

Fig. 18. Tangential FRF of the stator yoke due to tangential unit wave force of even orders from r=0 to r=14.

it possible to catch longitudinal modes of orders up to $n = 4$. The stator lamination is M400-50A for which the density is 7650 kg/m^3 and the orthotropic elastic properties are listed in Table II.

After the numerical resolution, 500 modes are found under 1500 Hz but only a few of them will potentially have an influence on the radial vibration level. Some of the main structural modes of the stator are illustrated in Fig. 16, and their associated natural frequencies are given in Table III. The natural frequencies are very low due to the large size of the machine and can be excited by magnetic force harmonics due to the interaction between rotor salient poles and stator slots, saturation and PWM effects. Each mode is characterized by the nature of the deflection – either radial or torsional – and the pair (m, n), where m is the circumferential order and n is the axial order of the deflection. The radial modes directly deflect the stator yoke while torsional modes may cause radial vibrations due to tooth bending modes.

As mentioned before, only the radial modes with "low" circumferential orders m will generally have an influence of noise and vibrations [11], particularly the modes (0,0), (2,0) and (4,0), as the vibration level decreases as a function of $1/m^4$. However, for this type of machine with relatively large diameter and relatively thin yoke, it may be necessary to consider circumferential orders up to m = 14 (pole number), especially because the PWM introduces magnetic forces of order $m = 0$ and $m = 2p$ (p is pole pair number). The magnetic forces are assumed to be balanced (no eccentricity, and circular stator bore radius) and only the circumferential modes of even orders can be excited. Torsional modes generally induce radial vibrations of lower magnitude and are usually neglected, but they are included here in the computation process.

C. Frequency Response Function (FRF)

Unit magnitude rotating force waves (f, r) are successively applied at the stator tooth tips, first in the radial direction and secondly in the tangential one, with

$r \in$ {-14, -12, -10, -8, -6, -4, -2, 0, 2, 4, 6, 8, 10, 12, 14}

and

$$f \in \{0 : 10 \text{ Hz} : 2000 \text{ Hz}\}.$$

The applied force wave is uniform over the axial direction, as the machine is not skewed. Negative wavenumbers account for different rotating force wave directions in order to model pulsating force waves that can be present in magnetic excitations, especially in case of non-sinusoidal supply. The damping is fixed to 2% for all FRF.

The resulting FRF calculations are shown in Fig. 17 and Fig. 18. They represent the radial displacement of the stator yoke per force unit expressed in dB to better see the resonance effect. The radial and torsional structural modes are represented in black and red dotted vertical lines, respectively. One can see that both radial and tangential force waves can generate a radial deflection and potentially excite the radial structural modes, contrary to what is generally assumed. In fact, the radial forces may also excite structural modes of the yoke driven by tooth torsional modes, as shown on Fig. 17, where the excitation with $r = 2$ excites the tooth torsional mode (2,0). Concerning the tangential FRF in Fig. 18, one can see that tangential excitations of wavenumber $r = 0$ excite the tooth torsional modes $(0, n)$, while tangential excitations with $r > 0$ resonate with the radial modes of same order, giving the same FRF as for radial excitations.

Both figures confirm the resonance phenomenon between magnetic excitation and structural modes. It means that the displacement level is strongly amplified when the excitation wavenumber r is the same as the mode circumferential order m and the excitation frequency f is close to the natural frequency

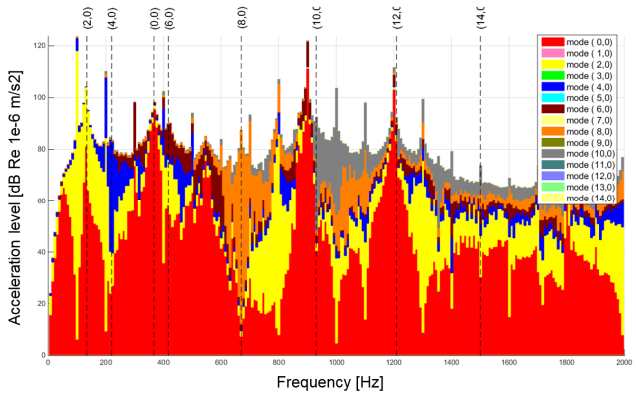

Fig. 19. Vibration spectrum (acceleration of stator external yoke).

f_m of the mode. Other peaks of lower magnitude are shown on the FRF. They are due to the resonance with the structural modes with same circumferential order m and non-null axial order ($n \geq 1$). The higher is the axial order n, the lower is the resonance peak. The FRF found for r= 12 and r= 14 are much lower than the others, which is probably due to the high stiffness of the stator structure under high wavenumber excitation.

D. Electromagnetic Vibration Synthesis (EVS)

The vibration spectrum is shown in Fig. 19, where the contribution of structural modes has been enlightened. The highest harmonics of vibrations are mainly due to the excitation of the radial structural modes m=0 (in red) and m=2 (in yellow). The two red peaks at f = 900 Hz and f = 1200 Hz ($f_{PWM} \pm 3f_s$) are produced as a result of converter-fed operation. As shown in Fig. 4, the current waveform contains relatively large harmonics at $f_{PWM} \pm 2f_s$. As a result, flux density harmonics are created at the same frequencies, having the same spatial order as the pole pair number, i.e. ($f_{PWM} \pm 2f_s, p$). The interaction between these flux harmonics and main flux density component, i.e. (f_s, p), produces force waves at ($f_{PWM} \pm 3f_s$, 0) and ($f_{PWM} \pm 3f_s$, 2 p). As shown by the FRF of wavenumber 2 p=14, forces of wavenumber 2 p cannot generate significant vibration. However, force harmonics of wavenumber $r = 0$ have significant magnitude and also seem to excite the structural mode (0,4) at 876 Hz. One can observe that every mode $(0, n)$ is excited by these types of magnetic forces. Besides, PWM harmonics create other vibration harmonics at any frequency equal to $f_{PWM} \pm kf_s$ where k is an odd integer. They consequently have a considerable impact on the machine vibrations as they increase both harmonic content and vibrations overall level.

VI. Conclusion

In this paper, converter-fed operation of a hydrogenerator is investigated. It is shown that the temporal harmonics produced by switching can be seen in the flux density and radial force waves, as well as rotor field current and torque. It is concluded that the characteristics of the lowest non-zero modes of vibration (e.g. 2nd and 4th) are not considerably affected by converter-fed operation. In contrast, it is revealed the 0th mode of vibration is strongly intensified as a result of additional harmonics produced by PWM converter.

References

[1] M. Valavi, A. Nysveen, "Variable-speed operation of hydropower plants: past, present, and future," in *Proc. ICEM*, 2016, pp. 640-646.

[2] "Modeling and analysis of value of advanced pumped storage hydropower in the United States," Argonne National Laboratory, 2014.

[3] P. K. Steimer, O. Senturk, S. Aubert, S. Linder, "Converter-fed synchronous machines for pumped hydro storage plants," in *Proc. ECCE*, 2014, pp. 4561-4567.

[4] "Guide for preliminary design and specification of hydro stations with HVDC unit connected generators," CIGRE report, August 1997.

[5] "Status report on variable speed operation in small hydropower," Energie publications, 2000.

[6] R. J Kerkman, T. A. Lipo, W. G. Newman, J. E. Thirkell, "An inquiry into adjustable speed operation of a pumped hydro plant- part 1: machine design and performance," *IEEE Trans. Power Apparatus and Systems*, pp. 1828-1837, September/October 1980.

[7] M. Valavi, A. Nysveen, R. Nilsen, "Investigation of magnetic field and radial force harmonics in a hydrogenerator connected to a three-level NPC converter," to be presented at *IECON*, 2017.

[8] B. Cassoret, J. P. Lecointe, and J. F. Brudny, *Power Electronics and Motor Drives*. Boca Raton, FL, USA: CRC Press, 2011.

[9] E. Devillers, M. Hecquet, J. Le Besnerais and M. Régniez, "Tangential effects on magnetic vibrations and acoustic noise of induction machines using subdomain method and electromagnetic vibration synthesis", in *Proc. IEMDC*, 2017.

[10] MANATEE (Magnetic Acoustic Noise Analysis Tool for Electrical Engineering). Available at http://www.eomys.com.

[11] J. Le Besnerais, "Fast prediction of variable-speed acoustic noise and vibrations due to magnetic forces in electrical machines," in *Proc. ICEM*, 2016, pp. 2259-2265.